Sensors & Actuators: B. Chemical 281 (2019) 945–952

Contents lists available at ScienceDirect

Sensors and Actuators B: Chemical

journal homepage: www.elsevier.com/locate/snb

Exploiting sensor geometry for enhanced gas sensing properties of fluorinated carbon nanotubes under humid environment

C. Struzzi[a,b,*], M. Scardamaglia[a,c], J. Casanova-Chafer[d], R. Calavia[d], J.-F. Colomer[e], A. Kondyurin[c,f], M. Bilek[c], N. Britun[a], R. Snyders[a,g], E. Llobet[d,**], C. Bittencourt[a]

[a] Chimie des Interactions Plasma-Surface, CIRMAP, University of Mons, 7000, Mons, Belgium
[b] MAX IV Laboratory, University of Lund, 22100, Lund, Sweden
[c] Applied and Plasma Physics Group, Physics Department, University of Sydney, Sydney, Australia
[d] MINOS Group, Universitat Rovira i Virgili, Tarragona, Spain
[e] Research Group on Carbon Nanostructures (CARBONNAGe), University of Namur, 5000, Namur, Belgium
[f] Farm, Ewingar, 2469, NSW, Australia
[g] Materia Nova Research Center, 7000, Mons, Belgium

ARTICLE INFO

Keywords:
Fluorinated carbon nanotubes
Sensing response to NO_2 and NH_3
Room temperature gas sensors
Increased response reproducibility under humid conditions

ABSTRACT

Modification of the surface electronic properties of vertically aligned and randomly distributed carbon nanotubes and the hydrophobic character after exposure to Ar:F_2 and CF_4 plasma are exploited to optimize the sensing characteristics of these materials. The sensing properties of fluorinated carbon nanotubes are disclosed by probing their stability and responsiveness towards the detection of two selected pollutants such as nitrogen dioxide and ammonia (NO_2 and NH_3). The effects of both humidity level and geometry of the sensing layer are assessed. It is demonstrated that fluorination, by increasing the surface hydrophobicity, results in increased response reproducibility and enhanced sensor response towards NH_3 when using vertically aligned carbon nanotubes.

1. Introduction

Nitrogen dioxide (NO_2) and ammonia (NH_3) are critical air pollutants, the former resulting from combustion or automotive emissions while the second is a dangerous analyte that has both natural and industrial derivation. In the perspective of real-time analysis, miniaturization and cost effectiveness, semiconducting metal oxide films, capacitive polymers and silicon devices have represented the most common active layers for detection of hazardous gases [1,2]. More recently, the implementation of carbon allotropes in gas sensor technology has been suggested to meet the demand of improved criteria as sensitivity, selectivity, long-term stability and reduced fabrication cost [3–7]. Among the peculiar characteristics of carbon nanomaterials, their high aspect ratio is a key aspect promoting them as potentially excellent sensing platforms as the whole surface is involved in the process leading to a maximization of the sensing performance upon exposure to adsorbates. The introduction of active sites on the pristine carbon structure has been explored largely to boost the reactivity to gases while improving both the selectivity and the sensitivity during the detection of hazardous molecules [8,9]. Devices based on doped graphene have already shown competitive efficiency in detecting glucose [10], thus enlarging its applicability in bio-sensing technology as well. The deposition of metal [6,11,12] and metal oxide nanoparticles on carbon allotropes [13] has been proposed to improve their sensing performances. In a recent study, quinoxaline-walled thioether-legged deep cavitand functionalized multiwall carbon nanotubes have shown unprecedented sensitivity towards traces of benzene vapours [14]. However, the sensor response toward aromatic volatile organic compounds diminished as the relative humidity in the gas flow was increased due to the oxygenated defective sites at the nanotubes surface.

For optimal environmental monitoring, the humidity effects must be assessed in order to extend the use of a performant sensing device to humid working environments as well. In this respect, fluorination of carbon nanomaterials could represent a valuable solution to hinder the moisture interference as the polarity of the covalent C–F bond favours an enhanced hydrophobic character [15]. Besides the hydrophobicity, the tuning of the density of states in fluorinated carbon nanomaterials and the thermal stability of the F–C bond play a key role in several

* Corresponding author at: Chimie des Interactions Plasma-Surface, CIRMAP, University of Mons, 7000, Mons, Belgium.
** Corresponding author.
E-mail addresses: claudia.struzzi@maxiv.lu.se (C. Struzzi), eduard.llobet@urv.cat (E. Llobet).

https://doi.org/10.1016/j.snb.2018.10.159
Received 28 June 2018; Received in revised form 23 October 2018; Accepted 30 October 2018
Available online 08 November 2018
0925-4005/

application fields [16], including gas sensing experiments. The improved ambient and thermal stabilities of fluorine functionalities grafted at the carbon nanostructures surface promote such materials as potential room temperature sensing devices substituting graphene oxide or oxidized carbon nanotubes, whose performances as selective gas sensor can be compromised by the high response to variable relative humidity level and by the reduced electrical conductivity [17–19]. Recent measurements on fluorinated graphite have reported a good sensing response to several hundreds of ppm concentration of ammonia and nitrogen dioxide [20,21]. However, the sensing measurements of fluorinated carbon nanomaterials were only performed under controlled dry air, Ar or N_2 atmosphere, or in vacuum and these conditions do not reproduce the realistic working condition requested for a commercialized gas sensor.

In the present work, two fluorine-based gas precursors are used for the plasma fluorination of carbon nanotubes, namely Ar:F_2 and CF_4, since multiple fluorinated carbon groups, as CF_3, are also grafted at the carbon nanotubes surface when using the latter precursor [22,23]. After the fluorination, the carbon nanotubes are integrated in home-made chemical gas sensors platforms to address three main factors. Firstly, the possible role played by the different patterning of the fluorinated carbon sites obtained with the two plasma treatments is unravelled. Secondly, the influence of fluorine functionalities over the pristine sensor response is probed. Thirdly, the interference of humidity in the environment is addressed, as it represents the main drawback hindering the functionalized carbon-based sensing properties. The increased hydrophobicity of the carbon surfaces after fluorination is exploited, leading to an increased response reproducibility under variable humidity level. The sensing mechanism and the geometry of the sensing layer are also investigated showing an enhanced response when vertically aligned carbon nanotube forests are used as sensing layer compared to the randomly distributed, spaghetti-like nanotube mats due to the remarkable role played by the exposed tips in the vertical configuration of the forest.

2. Materials and methods

Vertically aligned carbon nanotubes (vCNT) are synthesized by catalytic chemical vapour deposition (CCVD) at atmospheric pressure using Fe nanoparticles as catalyst. More details on the synthesis can be found in previous reports [24,25]. The as-synthesized close-packed vCNT are well-aligned multiwalled carbon nanotubes of 150–200 μm length, a dozen walls are found on average. To fabricate spaghetti-like carbon nanotube mats with random distribution, the CNT powder (Nanocyl®, purity level 95%) is sonicated in isopropanol for 30 min and the CNT mat is obtained by drop casting the suspension on silicon wafers kept at T = 100 °C to facilitate solvent evaporation.

Fluorination of the CNT surface is achieved in a post-discharge of a microwave (MW) plasma reactor where the discharge is sustained in a quartz tube by a surface wave (surfaguide type) launcher. A SAIREM 6 kW pulsed microwave generator working at 2.45 GHz has been used [26]. The gas flow rate is set to 100 sccm for both CF_4 and for the Ar:F_2 mixture (95:5) giving a post-discharge pressure of about 1 mbar. The power is maintained to 0.55 kW and the frequency to 1 kHz with a duty ratio fixed to 80%. The samples are placed on a supporting stage at a distance of 30 cm from the end of the discharge tube. To obtain different fluorination yields, the exposure time is changed ranging from 2.5 to 20 min. No changes are observed in the weight and in the structure of the carbon nanotubes.

The contact angle measurements are conducted using the static sessile drop method based on a direct optical measurement. The experimental set-up consists of a movable horizontal stage where the sample is placed, an automatized micrometre pipette system to generate the few microliter liquid drop of Milli-Q water, and an integrated camera for acquisition of real time images. Several points over each sample surface are analysed for accuracy and reproducibility during the drop profile analysis.

The photoemission studies are carried out at the Soft X-ray beamline of the Australian Synchrotron in Melbourne. The valence band spectra are collected using a photon energy of 110 eV, while a photon energy of 800 eV is used for the acquisition of the F1 s core levels to enhance the surface sensitivity. Spectroscopy data are acquired in normal emission geometry. The carbon (C) and fluorine (F) K-edge NEXAFS spectra are obtained in the partial electron yield mode. The NEXAFS measurements are performed by positioning the samples at the magic angle, that is the angle at which the measured intensity distribution is independent from the molecular orientation.

The chemical composition of the fluorinated samples after the sensing measurements is probed by using a VERSAPROBE PHI 5000 from Physical Electronics, equipped with a monochromatic Al Kα X-ray source. The experimental geometry of the data collection allows the analysis of carbon nanotube surface with an energy resolution better than 0.5 eV. For the compensation of built-up charge on the sample surface during the measurements, a dual beam charge neutralization composed of an electron gun ($\approx$1 eV) and an Ar ion gun ($\leq$10 eV) is used.

For the sensing measurements, a customization of the device is used to prepare the sensors. A commercial Ag paste (Heraeus AD 1688-06) is employed to glue a screen-printed Pt resistor, working as a heater, on the backside of the sample. Pt wires connect the heater resistor to a PCB board that can be plugged into the sensor test chamber through soldered connections. Parallel silver electrodes are realized on top of the sample surface and connected to the PCB board through Pt wires. At each step, the contacts are cured at 100 °C for 30 min in the oven.

The measurement rig comprises a set of computer-controlled mass flow meters and electro-valve systems to ensure reproducible concentrations of the gases that are delivered to the miniaturized Teflon chamber (35 mL). The DC resistance of the sensors is continuously measured with an Agilent 34,972 A multimeter. In a typical measurement cycle, pure dry air (Air Products) is flowed through the chamber until the sample resistance is stabilized, corresponding to a constant baseline R_0. Successively, given concentrations of NO_2 or NH_3 vapours are fed into the test chamber and kept flowing during the chosen exposure time, that is usually fixed to 10 min unless otherwise specified. The total flow is fixed to 100 sccm during the detection and recovery phases. During the detection time, the samples are kept at room temperature. After the detection measurements, the gas flow is switched again to pure dry air and the samples are allowed to re-stabilize to the room temperature baseline resistance. The relative humidity (RH) is constantly monitored using a thermo-hygrometer ICT-7 M from Ecological Sensors and Systems (ES&S). This sensor is located at the output of the test chamber recording both temperature and ambient moisture. It is considered dry condition when a residual amount of about RH = 4 ± 1% is measured. Under humid conditions, a specific amount of water in mg/h is introduced in the test chamber using a dedicated liquid mass flow system (Environics series 4000), which allowed generating humidified gas mixtures at different moisture levels.

The operational principle of resistive sensing devices consists of the variation of the electrical resistivity as a result of the adsorption of gas molecules on the sensor surface. The measurement of the resistance is continuously running, thus allowing a real-time acquisition of its variation from the initial value, which is the sensor baseline resistance R_0, during a complete exposure cycle. The sensor response, expressed as a percentage, is defined (unless otherwise specified) as the normalized resistance variation, $|(R_f - R_0)/R_0| \times 100$, where R_f is the resistance value measured when the gas flow is switched to pure air. The sign of the resistance variation depends on the type of semiconducting layer (n- or p- type depending on the electron or hole doping) and on the donor/acceptor behaviour of the detected molecule. Since holes are the major charge carriers in fluorinated carbon nanotubes, the fluorinated surface behaves as a p-type semiconductor.

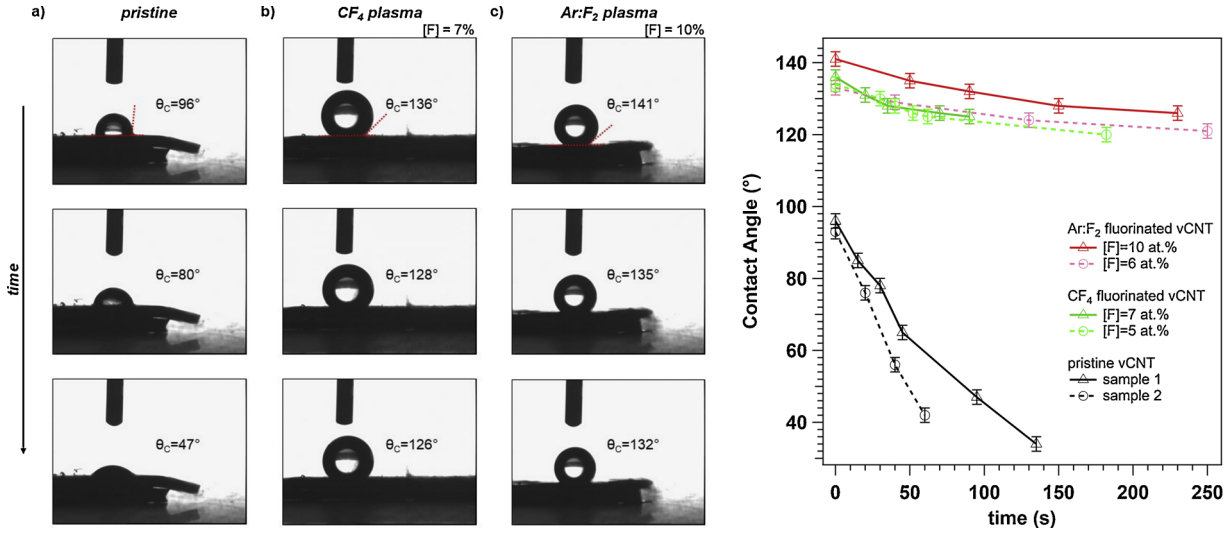

Fig. 1. (Left) Contact angle measurements on vertically aligned carbon nanotubes are shown for increasing fluorine content. The pictures along each column illustrate the time evolution of the water droplet. (Right) Contact angle values are acquired at increasing time to trace the water droplet evolution on two pristine samples (black curves) and on different plasma fluorinated samples, Ar:F_2 and CF_4, with various fluorine content (red and green curves) (For interpretation of the references to colour in this figure legend, the reader is referred to the web version of this article).

3. Results and discussion

The wettability of pristine and fluorinated vCNT is probed by measuring the contact angle at the interface with a liquid Milli-Q water drop, as shown on the left side of Fig. 1 (upper row). The initial contact angle value of pristine vCNT (θ_C = 96°) gradually rises with increasing fluorine content up to a value of θ_C = 141° for 10 at.% of F, thus reflecting the increased hydrophobic character introduced through the functionalization. The wettability is strongly dictated by the oriented dipole-dipole interactions in partially fluorinated vCNT (first row, left side of Fig. 1). The successive rows in Fig. 1 (left) correspond to the time evolution of the water droplet, each picture is collected after 30 s from the corresponding previous image. The variation of the contact angle decay rate of the pristine and functionalized samples indicates a different impedance of water diffusion into the nanotube forests. The water droplet deposited on the pristine surface is not stable and penetrates the forest, this process is further facilitated by the presence of voids on a submicron scale within the vCNT. On the contrary, the fluorinated carbon nanotubes show only a moderate reduction of the contact angle values exhibiting a higher stability with time for increasing fluorine yield at the surface. Additional data showing the contact angle trends with time for other pristine and fluorinated samples are shown on the right side of Fig. 1.

In correspondence to the remarkable changes in the surface energy induced by the fluorination, the nature of the pristine electronic properties is also largely modified. The valence band spectra are outlined for each sample in Fig. 2a. The grafting of fluorine atoms on the vCNT surface provokes a strong quenching of the C-C π states at 3 eV in concomitance with the suppression of the density of states near the Fermi level and the appearance of an intense contribution at about 10 eV, associated to the F2p-like states, which dominates the spectrum [25]. The F1 s core level spectra are shown in Fig. 2b. Interestingly, the F1 s core level acquired on the CF_4 plasma fluorinated sample shift towards higher binding energy values with respect to the Ar:F_2 plasma

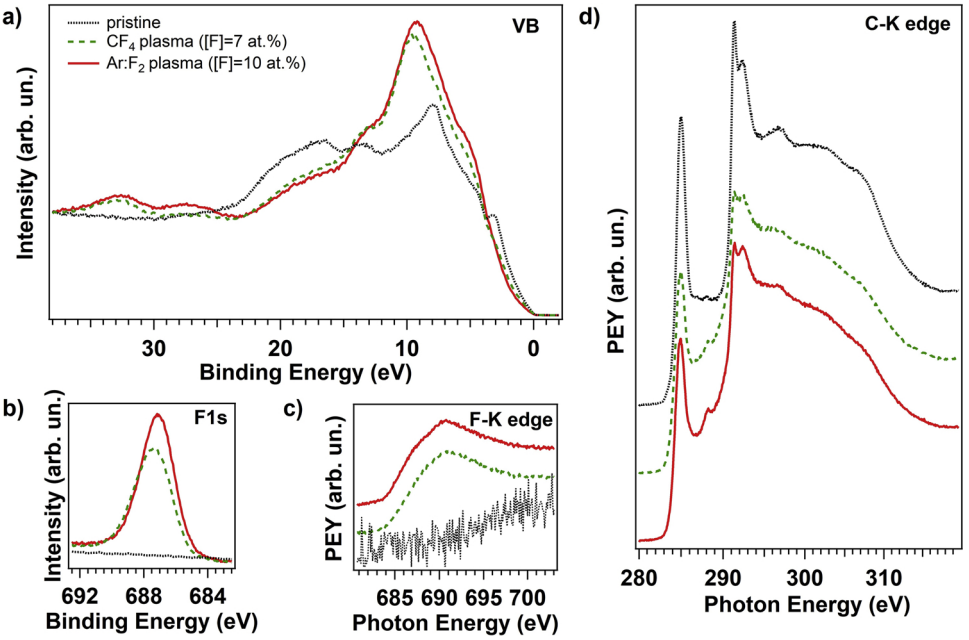

Fig. 2. Synchrotron-based measurements are performed on pristine (black dotted line) and on functionalized vCNT using different gas precursors. The fluorine contents are 7 and 10 at.% for the green dotted and red curves, respectively. Photoemission data are collected on the valence band (a) and the F1 s core level (b). Absorption spectra are shown for the F–K edge (c) and C–K edge (d). (For interpretation of the references to colour in this figure legend, the reader is referred to the web version of this article).

fluorinated vCNT, in line with the shift observed in the F2p-like states in the respective valence band spectrum. This shift is associated to the diverse chemical environment introduced at the surface by the multiple fluorinated carbon functionalities grafted on the vCNT [22].

The absorption spectra at the F–K and C–K edges are reported in Fig. 2c and d, respectively. The F–K edge signatures display broad structures composed of resonances at about 688 and 690 eV that are accompanied by weaker contributions at their sides, indicating dissimilar coordination for the fluorine atoms after both plasma treatments [23]. The large features at photon energy higher than 688 eV correspond to excitation from the F1 s to σ^* states due to the covalent interaction between fluorine and carbon atoms [27]. On the contrary, the resonances of π^* character are located at lower photon energies and they are associated to the interaction of fluorine with carbon atoms in the local vicinity of C–F groups (686 eV) [28].

The signals in the C–K edge can be divided into π and σ resonances. The absorption intensity associated to the transition from the C1 s level to the unoccupied π^* states (285 eV) decreases after the functionalization. The covalent C–F bond formation is confirmed by the peak at 288 eV increasing in intensity with higher fluorine content. The states corresponding to the transition from C1 s to σ^* suggest a limited extent of C–F bond formation with σ symmetry, thus supporting the evidence that the carbon nanotube structure is not destroyed by the plasma but it preserves the sp^2 character.

Pristine and fluorinated vCNT are then used as sensing layers for NO_2 and NH_3 detection at the ppm concentration range to test whether the fluorine functionalities affect the pristine sensor response for variable humidity level. The use of Ar:F_2 and CF_4 gas precursor for the plasma fluorination allows understanding the eventual role played by the multiple fluorinated carbon groups, as CF_3, during sensing mechanism as these species are mainly produced on the carbon nanotubes surface when using the CF_4 plasma [22,23].

The sensing experiments presented hereafter are performed at room temperature due to the observed desorption process of the functionalities, which is already activated when annealing at T = 250 °C in UHV condition, as shown in Fig. S1 in Supporting information where spectroscopic and absorption data are acquired as a function of the annealing temperature.

Due to the vertical geometry of the sensors the electrodes are placed on top of the densely packed nanotubes, therefore the sensing properties are only due to the intrinsic properties of the carbon nanotubes, *i.e.* the substrate is not playing any role.

The typical sensor response curves are illustrated in Fig. 3 where the normalized response (left axis) is plotted as a function of exposure time (bottom axis) to various analyte concentrations (right axis) at dry condition, corresponding to RH = 5% humidity level. The black dotted curves in Fig. 3 correspond to the pristine vCNT sensor (no trace of oxygen detectable on the surface), the red curves are obtained from the fluorinated vCNT using Ar:F_2 plasma, while the sensing responses of the CF_4 plasma functionalized sample are depicted as green dotted curves. The fluorine concentrations on these two samples are evaluated by XPS immediately after the fluorination process: 15 at.% of fluorine and about 2.5 at.% of oxygen contents are detected on the surface of the Ar:F_2 fluorinated sample (10 min of plasma treatment), while a fluorine concentration of 16 at.% and 1.5 at.% of oxygen is found after CF_4 plasma (10 min of plasma treatment).

All samples behave as p-type materials due to the increased conductivity (reduced resistance) when exposed to NO_2, and *vice versa* a decrease in the conductivity is measured when NH_3 flows in the chamber. The pristine vCNT sensor shows a fast reaction to the presence of nitrogen dioxide, but the response is characterized by a low recovery time once the gas flow is switched to pure air. On the contrary, the pristine sample is not sensitive to the ammonia molecule, neither at higher concentration (100 ppm), in agreement with previous results where the pristine nanotubes showed sensitivity to ammonia only after an intensive oxygen plasma treatment [29]. The fluorinated vCNT using Ar:F_2 plasma exhibits a good response to both gases with an improved recovery time for the release of NO_2 molecule once the gas flow is switched to pure air. The instantaneous response of all vCNT sensors can be attributed to both the full exposure of the nanotube surface area to the two chemical environments and to the mobility of the charge carriers leading to a fast transmission of the signal. Additionally, a better recovery (about 50%) of the fluorinated sensors is observed after NO_2 detection with respect to NH_3 experiments. The slow recovery process after ammonia exposure suggests a slower molecular desorption of NH_3 from the nanotube due to a stronger chemical interaction occurring mainly between the fluorinated sites on the carbon surface and the ammonia molecules. Further, diffusion process may occur into the three-dimensional porous architecture of the vCNT forest and additional external energy would be consequently required, for example in the form of heating treatment, to favour the release of this pollutant. However, a heating treatment would promote the desorption process of fluorine atoms from the surface in the present case (see Fig. S1 in Supporting information).

Compared to the absence of ammonia detection for the pristine sample, the fluorinated carbon nanotubes exhibit stronger adsorption capacities and better sensing properties. The improvement in the sensing performance of fluorinated vCNT is associated to both the strong polarity and the reactivity of F atoms in interacting with the hydrogen atoms of the analyte resulting in hydrogen bonding interactions. On the other side, also the interaction with NO_2 is not negligible considering the incomplete resistance baseline recovery at room temperature, analogous to previous results where a rather strong interaction was found [29]. This observation implies that complete NO_2 desorption is

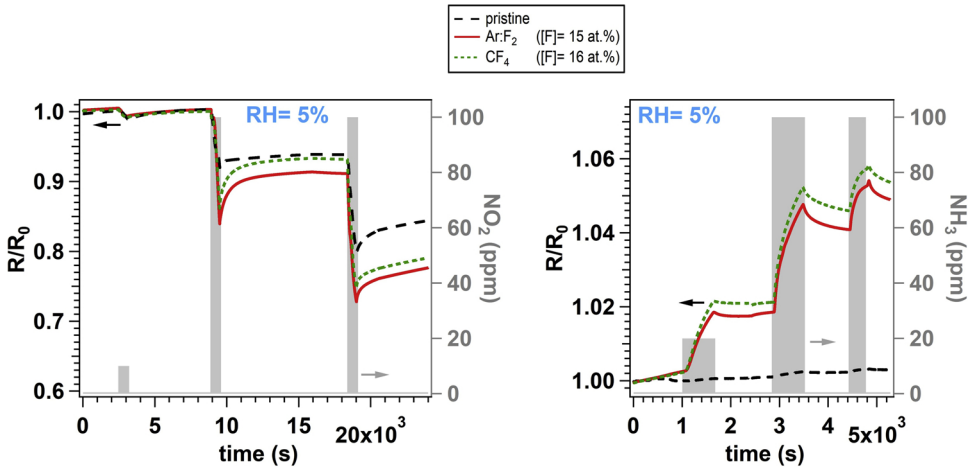

Fig. 3. The typical response and recovery curves of pristine and fluorinated vCNT sensors are shown for low (10 or 20 ppm) and high (100 ppm) concentration of the two analytes shown as grey bar (right axis). The measured resistance curves are normalized to the relative baseline value R_0 of each sensor (left axis). The experimental data are collected with a relative humidity level of RH = 5%.

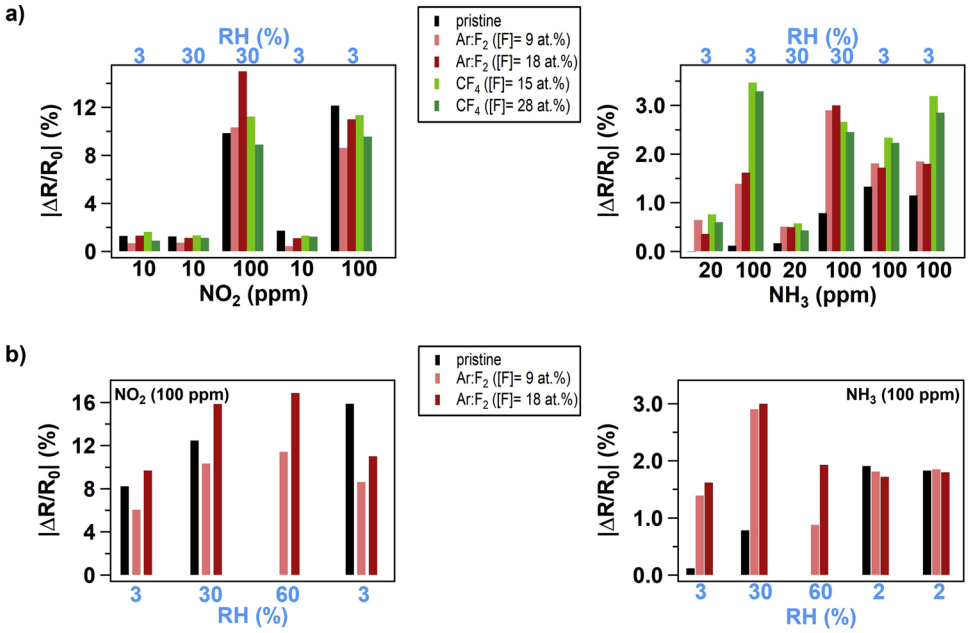

Fig. 4. a) The relative sensor responses to low and high concentrations of NO_2 and NH_3 are shown for pristine and fluorinated vCNT with different fluorination yields, as indicated in the legend, and for switching humidity levels (RH = 3/30%). b) The relative sensor response to 100 ppm of NO_2 and NH_3 at variable humidity levels (RH) is shown for pristine and Ar:F_2 plasma fluorinated vCNT with different fluorination yields, as indicated in the legend.

not achievable at room temperature and that stronger interaction than Van der Waals interaction with the carbon nanotubes, as chemisorption, cannot be ruled out for this analyte. At the same time, the diffusion of NO_2 down the nanotube forest may also hinder the complete release of the analyte during recovery phase.

The increased hydrophobicity of the carbon surfaces after fluorination is exploited to probe the gas sensing reproducibility under variable humidity level and the relative sensor responses are shown in Fig. 4. The response values are calculated over 10 min of exposure and expressed as a percentage.

In Fig. 4a, the moisture effect is analysed for the pristine and for the differently plasma fluorinated vCNT (Ar:F_2 and CF_4 plasma) thus allowing the investigation of a possible dependence of the sensor response on the functionalization used. In this experiment, the humidity level is switched from RH = 3% to RH = 30% while measuring the responses to low and high concentrations of NO_2 and NH_3. All sensor responses to traces of nitrogen dioxide are near to three times higher than the detection capability towards similar concentrations of ammonia. The response of pristine nanotubes towards NH_3 is rather dependent on the humidity content, increasing with increasing concentration of water molecules in the environment. When humidity is diminished from 30% to 3%, the response to ammonia remains almost identical to the one for 30% in the pristine sample. Most probably, the adsorbed moisture penetrated deeper in the forest (as observed during contact angle measurements) and the water contamination of the pristine surface could lead to a charge redistribution affecting the current through the layer. On the other hand, when the surface of the forest is fluorinated, the hydrophobic character is significantly higher than that of the pristine vCNT surface resulting in a reproducible response of the fluorinated films under variable humidity levels.

Variations in the amount of fluorine functionalities grafted on the sample surface does not impact the sensor response to NO_2. The response of fluorinated vCNT sensors towards nitrogen dioxide is, in essence, the same as that measured with the pristine samples in line with the fluorination content affecting less than a third of the sample surfaces in all cases. This result suggests that reducing the interaction of carbon nanotubes with water *via* fluorination does not alter their interaction with NO_2, thus promoting the plasma fluorination as a valuable substitution to O_2 plasma treatment and pioneering the anchoring of recognition elements to improve selectivity and sensitivity, similarly to previous works [14,30].

In addition, the particular gas precursor used during fluorination does not have a strong effect on the sensor performance, therefore the relative response can be measured within a wider humidity range, from dry air (RH = 3%) up to RH = 60%, testing one pristine and two Ar:F_2 plasma fluorinated samples, as illustrated in Fig. 4b. The strong influence of the moisture concentration on the pristine sample response (black bars) is further confirmed: the resistance variation continuously raises upon successive nitrogen dioxide exposures and an emerging response to NH_3 is detected under humid condition, though the pristine sample did not show sensitivity to ammonia during the first measurements in dry condition. No recovery of the starting pristine performance is observed in the successive measurements under dry air, suggesting that the humidity can be considered as the primary interfering analyte responsible for the performance deterioration with time in this sensor. Once exposed to water, the active material changes dramatically the response intensity to the pollutants and there is a strong memory effect when exposed again to a flow of dry air, *i.e.* the response remains altered as if humidity was still present due to the penetration of water molecules deeply in the carbon nanotubes forest. This memory effect prevents the use of such a sensor in a scenario in which ambient humidity may change, given the impossibility of calibrating the sensor.

In contrast to the pristine vCNT sensor, when the concentration of water molecules is increased to 30%, the fluorinated vCNT response is enhanced, implying that the presence of water does not block the interaction between adsorbed molecules and the vCNT. Although the response is affected by humidity being different under dry or humid conditions due to the presence of water molecules on top of the forest, fluorinated vCNT do not experience the memory effect. The response nearly returns to the original value as soon as the dry condition is re-established and it remains unvaried during the successive measurements at RH = 2–3%, suggesting that the adsorbed water molecules are easily evacuated without heating the sensors or without the necessity of using an inert gas flow. As a result, sensor response becomes reproducible and a humidity-calibrated response could be possible, *e.g.* including a humidity sensor.

Reproducible results are obtained after repeated sensing measurements over time indicating good sensor performance when working in ambient condition. Nevertheless, the relative response measured with fluorinated vCNT should be further improved to reach the high level of detection measured in metal decorated carbon nanotubes, especially when detecting ammonia [6,11,12]. However, the response of the

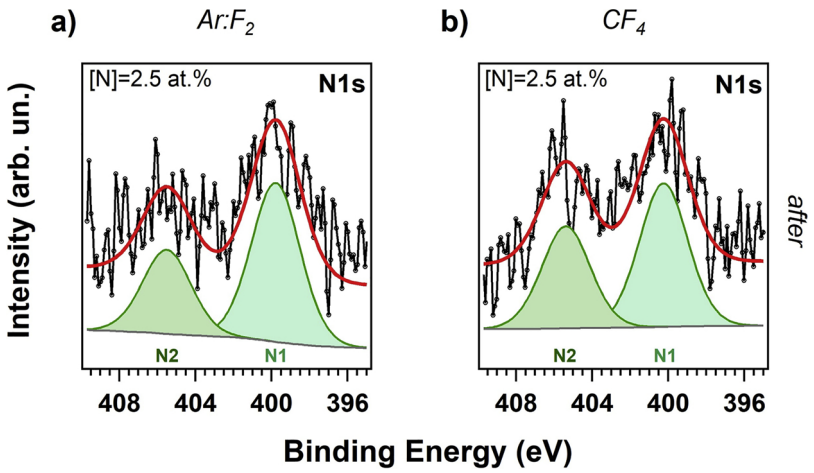

Fig. 5. The N1 s core level signals are measured after implementing the functionalized samples in a gas sensing device (after test gas exposure). The N1 s signal is only detected after the sensing measurements and exclusively on fluorinated vCNT.

fluorinated vertically aligned carbon nanotubes to NH_3 is higher compared with recent results from fluorinated graphene layers [20], where a maximal response of 11% on detection of 10,000 ppm of NH_3 in argon atmosphere was achieved after more than 10 min of exposure and with a recovery time longer than 30 min. In the same experiment, the response decreased to 2% when a concentration of 600 ppm of ammonia was detected.

The sensor response, the selectivity to ammonia and the response reproducibility in humid environments have been demonstrated so far, showing a satisfactory performance of the plasma fluorinated sensors. To probe the effect of the sensing measurement on the chemical composition of the surface and determine the nature of the interaction with the target gases, the nitrogen content has been monitored by XPS. The N1 s core level signal is only detected after the sensing measurements and exclusively on fluorinated vCNT surface. In Fig. 5, the N1 s core level spectra are illustrated for the (a) Ar:F_2 sample (F concentration of 15 at.%) and for the (b) CF_4 plasma functionalized vCNT (F concentration of 16 at.%). The nitrogen concentration evaluated by XPS is 2.5 at.% in both samples. The N1 s spectra are composed of two main components: N1 located around 400 eV and N2 near 406 eV binding energy. The former is commonly associated to amines [31] indicating the presence of NH_3 still adsorbed on the sample surface due to the higher interaction. The second component N2 is instead assigned to nitrogen dioxide molecules adsorbed on the nanotubes [32] likely as a pyridinic-*N*-oxide configuration [33] consistent with the presence of NO_2 on the vCNT surface. This observation is supported by the evidence of an increased uptake of oxygen on the surface after the sensor tests, in fact the oxygen concentrations increased from 2.5 (a) and 1 at.% (b) to 4 at.% in both cases.

The relative intensity of the two nitrogen components confirms that a higher amount of ammonia is adsorbed on the surface due to the stronger interaction with the fluorinated surface, in agreement also with the hindered recovery of the baseline during NH_3 sensing measurements.

According to theoretical calculations, the estimated adsorption energy of ammonia on pristine graphene is lower than the adsorption energy of nitrogen dioxide molecule [21,34,35], while the adsorption energy of NH_3 on fluorinated graphene is one order of magnitude higher than on the pristine surface [20,36]. Experimentally, we have measured a remarkably higher response to NO_2 with respect to the ammonia detection regardless of the fluorination as a consequence of the large charge transfer from the sensing layer to the analyte. This mechanism is sustained by the appearance of the LUMO state of nitrogen dioxide below the Dirac point [37] with a favoured orientation of the NO_2 molecule exhibiting the N atom pointing towards the F atom [38]. Reversely, the fluorination introduces a moderate sensing response towards ammonia in agreement with the predicted decrease in the distance between the analyte and the fluorinated carbon surface [39] that promotes a stronger interaction *via* the formation of hydrogen bonding as a result of a dipolar electrostatic interaction providing an enhanced charge transfer with the fluorinated carbon layer [20].

To further investigate the possible role played by the geometry of the sensing layer, randomly dispersed CNTs are tested. The carbon nanotubes are first drop-casted on a silicon wafer adopting a spaghetti-like distribution, the SEM images are shown in Fig. 6. Subsequently, the samples are inserted in the μ-wave plasma chamber and they are subjected to the plasma fluorination treatments. Finally, the contacts are realized on the surface following the experimental method used for the vCNT sensors and the sensing performance of the samples are tested in the same experimental chamber as used for the vCNT.

Under this arrangement, the sparse carbon nanotube mesh is not regular and it does not cover homogeneously the silicon surface therefore the response can be influenced by the substrate (extrinsic gas response). The response curves to variable NO_2 and NH_3 concentration

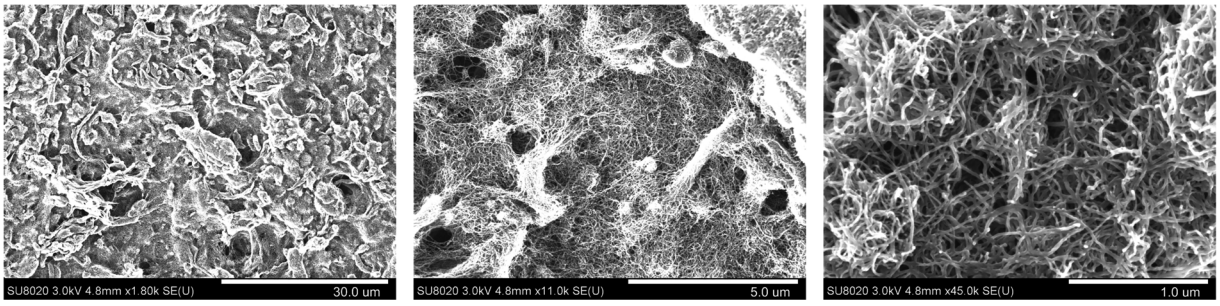

Fig. 6. The SEM images show the random distribution of the pristine multi-walled nanotubes drop-casted on a silicon wafer.

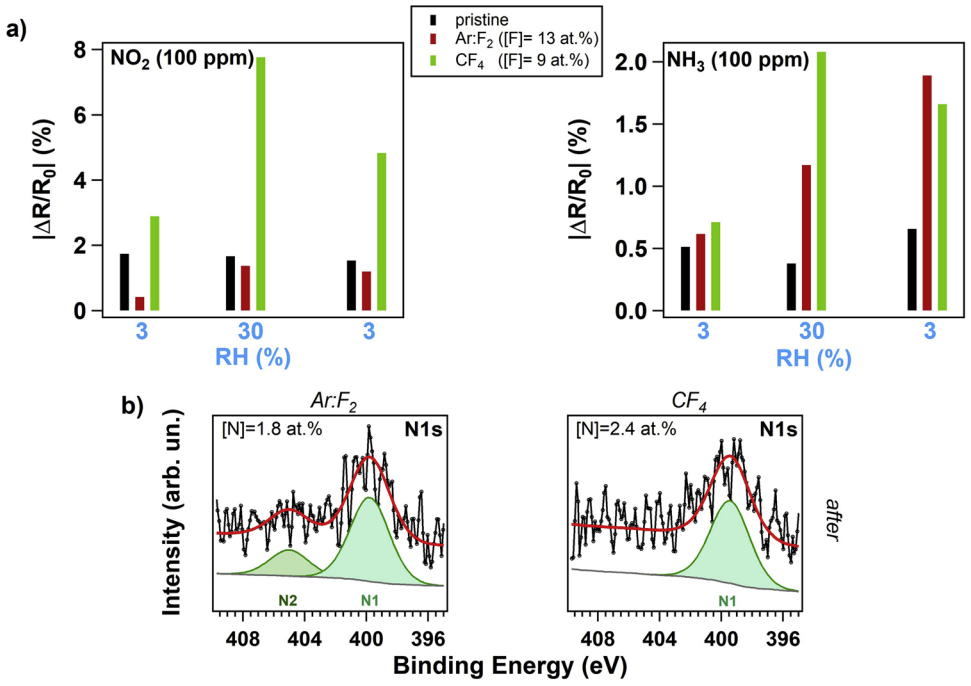

Fig. 7. a) The relative sensor response to 100 ppm of NO_2 and NH_3 is shown for pristine and fluorinated random CNT with different fluorination yield, as indicated in the legend, and switchable humidity level (RH = 3/30%). b) The N1 s core level signals are recorded after the sensing measurements performed using the fluorinated samples ($Ar:F_2$, left panel, and CF_4, right panel). The N1 s signal is detected only on fluorinated carbon nanotubes.

and different humidity levels are shown in Figs. S2 and S3 of the Supporting Information for pristine and plasma fluorinated samples.

The relative sensor responses are illustrated in Fig. 7a for pristine nanotubes (with an oxygen content of 4 at.%) and fluorinated samples containing a F concentration equal to 13 at.% ($Ar:F_2$ plasma) and 9 at.% (CF_4 plasma). Before the sensing measurements, the oxygen concentration on the two fluorinated sensors was 4.2 at.% and 1.5 at.%, respectively.

The response to NO_2 is notably lower than that of vCNT forest, confirming the remarkable role played by the tips that are directly exposed to the target gas in the vertical geometry. Furthermore, the change in the humidity concentration in the environment has a larger impact on the sensor performance for the sparse carbon nanotube mesh. The fluorination, especially using CF_4 plasma, seems to increase the influence of humidity level on the response towards NO_2 and NH_3 similarly to graphene oxide performance under wet condition [19]. The observed higher response of the CF_4 functionalized sample when RH = 30% is associated to an improved ammonia adsorption on the surface due to the presence of water molecules confined by the hydrophobic and highly dense fluorinated areas. Therefore, the inhomogeneous hydrophobic path could be a competitive counterpart leading to the production of an ionic current that facilitates local space charge creation. On the other side, the pristine random CNT samples are responsive to ammonia already under dry condition due to the presence of native oxygen on the surface.

The surface of the random CNT-based sensors is analysed by XPS after running the gas sensing measurements, the N1 s core level spectra are reported in Fig. 7b for the two fluorinated carbon nanotubes samples. The nitrogen signal is not detected on the pristine sensors, while the N1 s spectra are dominated by the N1 component in the plasma fluorinated nanotubes used for the sensing measurements. The N2 peak is visible in the $Ar:F_2$ plasma fluorinated sample (left panel): this observation combined with the slower recovery of the baseline during NO_2 measurements for this sensor (see Fig. S2 in Supporting information) confirms the assignment of the component to nitrogen dioxide molecule adsorbed on the surface. In analogy, the N2 component is not found on the CF_4 plasma fluorinated sensor (right panel) as the analyte desorbs faster from it (see Fig. S3 in Supporting information). The nitrogen uptake corresponds to a final concentration of 1.8 at.% for the $Ar:F_2$ plasma fluorinated sample and 2.4 at.% for the CF_4 plasma fluorinated sample, respectively.

4. Conclusion

The room temperature efficiency, the reliability and the high sensitivity towards detection of different gases have triggered great interest in the use of both pristine and functionalized carbon nanotubes as sensing layers. In the present work, a controlled plasma fluorination of carbon nanotubes is obtained using different fluorine-based gas precursors, namely $Ar:F_2$ and CF_4. The hydrophobicity of the pristine carbon nanotube forest is strongly increased and the water diffusion process inside the forest, observed for pristine vCNT, is largely impeded even at a fluorine content of only 7 at.%. The sensing response of the fluorinated carbon nanotube samples is investigated upon exposure to nitrogen dioxide and ammonia being representative for the opposite acceptor/donor behaviour. If from one side the fluorination does not alter the high response to NO_2 molecules, the improved sensing performance in detecting ammonia is associated to an increased interaction between NH_3 and the fluorinated carbon nanotubes surface, as confirmed by XPS measurements. A hydrogen bonding interaction favours the charge transfer to the fluorinated carbon-based sensor. The vertically aligned carbon nanotube forests show an enhanced sensor response compared to the planar distribution of spaghetti-like nanotubes. The vertical geometry is thus a preferable layer for the sensing platform due to the remarkable role played by the tips in the vCNT. Contrary to the pristine samples, improved response reproducibility in a variable ambient moisture levels is observed when testing fluorinated vCNT. This property makes fluorinated vCNT as potential material to be employed in practical commercial applications after sensor calibration: once the response changes *versus* variations in relative humidity are known, it will be possible to compensate this effect and implement them as room temperature gas detectors.

Acknowledgements

CS is grateful to the “Fonds pour la Formation à la Recherche dans l’Industrie et dans l’Agriculture” (F.R.I.A.) for financial support. CS also acknowledges the Stiftelsen för Strategisk Forskning (SSF) (Project no.

RMA15-0024). MS is FRS-FNRS post-doctoral researcher, J-FC and CB are Researcher Associates at the FRS-FNRS. The authors thank the Australian synchrotron radiation lightsource for the funding (grant no. AS161/SXR/10421) and the staff of the Soft X-Ray beamline. This work is supported by the Belgian Fund for Scientific Research (FRS-FNRS) under the FRFC contract "CHEMOGRAPHENE" (convention no. 2.4577.11). This research is also supported by a Marie Curie International Research Staff Exchange Scheme Fellowship within the 7th European Community Framework Programme "NanoCF" (grant agreement number: PIRSES-GA-2013-612577). Funded in part by MINECO and FEDER *via* grant no. TEC2015-71663-R and by AGAUR under grant no. 2017SGR 418. E.L. is supported by the Catalan institution for Research and Advanced Studies *via* the 2012 Edition of the ICREA Academia Award.

Declarations of interest: none.

Appendix A. Supplementary data

Supplementary material related to this article can be found, in the online version, at doi:https://doi.org/10.1016/j.snb.2018.10.159.

References

[1] X. Liu, S. Cheng, H. Liu, S. Hu, D. Zhang, H. Ning, A survey on gas sensing technology, Sensors (Switzerland) 12 (2012) 9635–9665, https://doi.org/10.3390/s120709635.

[2] J. Zhang, X. Liu, G. Neri, N. Pinna, Nanostructured materials for room-temperature gas sensors, Adv. Mater. 28 (2016) 795–831, https://doi.org/10.1002/adma.201503825.

[3] J. Kong, N.R. Franklin, C. Zhou, M.G. Chapline, S. Peng, K. Cho, H. Dai, Nanotube molecular wires as chemical sensors, Science 287 (2000) 622–625, https://doi.org/10.1126/science.287.5453.622.

[4] F. Schedin, A.K. Geim, S.V. Morozov, E.W. Hill, P. Blake, M.I. Katsnelson, K.S. Novoselov, Detection of individual gas molecules adsorbed on graphene, Nat. Mater. 6 (2007) 652–655, https://doi.org/10.1038/nmat1967.

[5] E. Llobet, Gas sensors using carbon nanomaterials: a review, Sens. Actuators B: Chem. 179 (2013) 32–45, https://doi.org/10.1016/j.snb.2012.11.014.

[6] P.R. Mudimela, M. Scardamaglia, O. González-León, N. Reckinger, R. Snyders, E. Llobet, C. Bittencourt, J.-F. Colomer, Gas sensing with gold-decorated vertically aligned carbon nanotubes, Beilstein J. Nanotechnol. 5 (2014) 910–918, https://doi.org/10.3762/bjnano.5.104.

[7] M. Meyyappan, Carbon nanotube-based chemical sensors, Small 12 (2016) 2118–2129, https://doi.org/10.1002/smll.201502555.

[8] J. Kong, M.G. Chapline, H. Dai, Functionalized carbon nanotubes for molecular hydrogen sensors, Adv. Mater. 13 (2001) 1384–1386, https://doi.org/10.1002/1521-4095(200109)13:18<1384::AID-ADMA1384>3.0.CO;2-8.

[9] P. Clément, A. Ramos, A. Lazaro, L. Molina-Luna, C. Bittencourt, D. Girbau, E. Llobet, Oxygen plasma treated carbon nanotubes for the wireless monitoring of nitrogen dioxide levels, Sens. Actuators B: Chem. 208 (2015) 444–449, https://doi.org/10.1016/j.snb.2014.11.059.

[10] G. Chen, Y. Liu, Y. Liu, Y. Tian, X. Zhang, Nitrogen and sulfur dual-doped graphene for glucose biosensor application, J. Electroanal. Chem. 738 (2015) 100–107, https://doi.org/10.1016/j.jelechem.2014.11.020.

[11] M. Penza, R. Rossi, M. Alvisi, E. Serra, Metal-modified and vertically aligned carbon nanotube sensors array for landfill gas monitoring applications, Nanotechnology 21 (2010) 105501, https://doi.org/10.1088/0957-4484/21/10/105501.

[12] Z. Zanolli, R. Leghrib, A. Felten, J.-J. Pireaux, E. Llobet, J.-C. Charlier, Gas sensing with Au-decorated carbon nanotubes, ACS Nano 5 (2011) 4592–4599, https://doi.org/10.1021/nn200294h.

[13] F. Rigoni, G. Drera, S. Pagliara, E. Perghem, C. Pintossi, A. Goldoni, L. Sangaletti, Gas sensing at the nanoscale: engineering SWCNT-ITO nano-heterojunctions for the selective detection of NH 3 and NO 2 target molecules, Nanotechnology 28 (2017) 035502, https://doi.org/10.1088/1361-6528/28/3/035502.

[14] P. Clément, S. Korom, C. Struzzi, E.J. Parra, C. Bittencourt, P. Ballester, E. Llobet, Deep cavitand self-assembled on Au NPs-MWCNT as highly sensitive benzene sensing interface, Adv. Funct. Mater. 25 (2015) 4011–4020, https://doi.org/10.1002/adfm.201501234.

[15] V. Mazánek, O. Jankovský, J. Luxa, D. Sedmidubský, Z. Janoušek, F. Šembera, M. Mikulics, Z. Sofer, Tuning of fluorine content in graphene: towards large-scale production of stoichiometric fluorographene, Nanoscale 7 (2015) 13646–13655, https://doi.org/10.1039/C5NR03243A.

[16] D.D. Chronopoulos, A. Bakandritsos, M. Pykal, R. Zbořil, M. Otyepka, Chemistry, properties, and applications of fluorographene, Appl. Mater. Today 9 (2017) 60–70, https://doi.org/10.1016/j.apmt.2017.05.004.

[17] S. Prezioso, F. Perrozzi, L. Giancaterini, C. Cantalini, E. Treossi, V. Palermo, M. Nardone, S. Santucci, L. Ottaviano, Graphene oxide as a practical solution to high sensitivity gas sensing, J. Phys. Chem. 117 (2013), https://doi.org/10.1021/jp3085759.

[18] H. Bi, K. Yin, X. Xie, J. Ji, S. Wan, L. Sun, M. Terrones, Ultrahigh humidity sensitivity of graphene oxide, Sci. Rep. 3 (2013) 1–7, https://doi.org/10.1038/srep02714.

[19] A. Bannov, J. Prášek, O. Jašek, L. Zajícková, Investigation of pristine graphite oxide as room-temperature chemiresistive ammonia gas sensing material, Sensors 17 (2017) 320, https://doi.org/10.3390/s17020320.

[20] M.V. Katkov, V.I. Sysoev, A.V. Gusel'nikov, I.P. Asanov, L.G. Bulusheva, A.V. Okotrub, A backside fluorine-functionalized graphene layer for ammonia detection, Phys. Chem. Chem. Phys. 17 (2015) 444–450, https://doi.org/10.1039/C4CP03552F.

[21] V.I. Sysoev, L.G. Bulusheva, I.P. Asanov, Y.V. Shubin, A.V. Okotrub, Thermally exfoliated fluorinated graphite for NO2 gas sensing, Phys. Status Solidi Basic Res. 253 (2016) 2492–2498, https://doi.org/10.1002/pssb.201600270.

[22] C. Struzzi, M. Scardamaglia, J.-F. Colomer, A. Verdini, L. Floreano, R. Snyders, C. Bittencourt, Fluorination of vertically aligned carbon nanotubes: from CF_4 plasma chemistry to surface functionalization, Beilstein J. Nanotechnol. 8 (2017) 1723–1733, https://doi.org/10.3762/bjnano.8.173.

[23] L.G. Bulusheva, Y.V. Fedoseeva, E. Flahaut, J. Rio, C.P. Ewels, V.O. Koroteev, G. Van Lier, D.V. Vyalikh, A.V. Okotrub, Effect of the fluorination technique on the surface-fluorination patterning of double-walled carbon nanotubes, Beilstein J. Nanotechnol. 8 (2017) 1688–1698, https://doi.org/10.3762/bjnano.8.169.

[24] M. Scardamaglia, M. Amati, B. Llorente, P. Mudimela, J.-F. Colomer, J. Ghijsen, C. Ewels, R. Snyders, L. Gregoratti, C. Bittencourt, Nitrogen ion casting on vertically aligned carbon nanotubes: tip and sidewall chemical modification, Carbon 77 (2014) 319–328, https://doi.org/10.1016/j.carbon.2014.05.035.

[25] C. Struzzi, M. Scardamaglia, A. Hemberg, L. Petaccia, J.F. Colomer, R. Snyders, C. Bittencourt, Plasma fluorination of vertically aligned carbon nanotubes: functionalization and thermal stability, Beilstein J. Nanotechnol. 6 (2015) 2263–2271, https://doi.org/10.3762/bjnano.6.232.

[26] T. Silva, N. Britun, T. Godfroid, R. Snyders, Optical characterization of a microwave pulsed discharge used for dissociation of CO2, Plasma Sources Sci. Technol. 23 (2014) 025009, https://doi.org/10.1088/0963-0252/23/2/025009.

[27] M. Klues, P. Jerabek, T. Breuer, M. Oehzelt, K. Hermann, R. Berger, G. Witte, Understanding the F 1s NEXAFS dichroism in fluorinated organic semiconductors, J. Phys. Chem. C 120 (2016) 12693–12705, https://doi.org/10.1021/acs.jpcc.6b04048.

[28] A.V. Okotrub, N.F. Yudanov, I.P. Asanov, D.V. Vyalikh, L.G. Bulusheva, Anisotropy of chemical bonding in semifluorinated graphite C2F revealed spectroscopy, ACS Nano 7 (2013) 65–74.

[29] R. Ionescu, E.H. Espinosa, E. Sotter, E. Llobet, X. Vilanova, X. Correig, A. Felten, C. Bittencourt, G. Van Lier, J.C. Charlier, J.J. Pireaux, Oxygen functionalisation of MWNT and their use as gas sensitive thick-film layers, Sens. Actuators B: Chem. 113 (2006) 36–46, https://doi.org/10.1016/j.snb.2005.02.020.

[30] A. Thamri, H. Baccar, C. Struzzi, C. Bittencourt, A. Abdelghani, E. Llobet, MHDA-functionalized multiwall carbon nanotubes for detecting non-aromatic VOCs, Sci. Rep. 6 (2016) 35130, https://doi.org/10.1038/srep35130.

[31] D. Zeng, X. Yu, Y. Zhan, L. Cao, X. Wu, B. Zhang, J. Huang, Z. Lin, F. Xie, W. Zhang, J. Chen, W. Xie, W. Mai, H. Meng, Insight into the nitrogen-doped carbon as oxygen reduction reaction catalyst: the choice of carbon/nitrogen source and active sites, Int. J. Hydrogen Energy 41 (2016) 8563–8575, https://doi.org/10.1016/j.ijhydene.2016.03.072.

[32] G. Ruiz-Soria, A. Pérez Paz, M. Sauer, D.J. Mowbray, P. Lacovig, M. Dalmiglio, S. Lizzit, K. Yanagi, A. Rubio, A. Goldoni, P. Ayala, T. Pichler, Revealing the adsorption mechanisms of nitroxides on ultrapure, metallicity-sorted carbon nanotubes, ACS Nano 8 (2014) 1375–1383, https://doi.org/10.1021/nn405114z.

[33] S. Kundu, W. Xia, W. Busser, M. Becker, D.A. Schmidt, M. Havenith, M. Muhler, The formation of nitrogen-containing functional groups on carbon nanotube surfaces: a quantitative XPS and TPD study, Phys. Chem. Chem. Phys. 12 (2010) 4351, https://doi.org/10.1039/b923651a.

[34] Y.-H. Zhang, Y.-B. Chen, K.-G. Zhou, C.-H. Liu, J. Zeng, H.-L. Zhang, Y. Peng, Improving gas sensing properties of graphene by introducing dopants and defects: a first-principles study, Nanotechnology 20 (2009) 185504, https://doi.org/10.1088/0957-4484/20/18/185504.

[35] S.S. Varghese, S. Lonkar, K.K. Singh, S. Swaminathan, A. Abdala, Recent advances in graphene based gas sensors, Sens. Actuators B: Chem. 218 (2015) 160–183, https://doi.org/10.1016/j.snb.2015.04.062.

[36] H. Zhang, L. Fan, H. Dong, P. Zhang, K. Nie, J. Zhong, Y. Li, J. Guo, X. Sun, Spectroscopic investigation of plasma-fluorinated monolayer graphene and application for gas sensing, ACS Appl. Mater. Interfaces 8 (2016) 8652–8661, https://doi.org/10.1021/acsami.5b11872.

[37] O. Leenaerts, B. Partoens, F.M. Peeters, Adsorption of H2O, NH3, CO, NO2, and NO on graphene: a first-principles study, Phys. Rev. B 77 (2008) 125416, , https://doi.org/10.1103/PhysRevB.77.125416.

[38] V.I. Sysoev, A.V. Okotrub, I.P. Asanov, P.N. Gevko, L.G. Bulusheva, Advantage of graphene fluorination instead of oxygenation for restorable adsorption of gaseous ammonia and nitrogen dioxide, Carbon 118 (2017) 225–232, https://doi.org/10.1016/j.carbon.2017.03.026.

[39] K.K. Tadi, S. Pal, T.N. Narayanan, Fluorographene based ultrasensitive ammonia sensor, Sci. Rep. 6 (2016) 25221, https://doi.org/10.1038/srep25221.